JOURNAL OF MATERIALS SCIENCE 32 (1997) 5593–5602

Fe–Zn phase formation in interstitial-free steels hot-dip galvanized at 450 °C

Part I *0.00 wt % Al–Zn baths*

C. E. JORDAN, A. R. MARDER
Department of Materials Science and Engineering, Lehigh University, Bethlehem, PA 18015, USA

Interstitial-free alloy steels containing various combinations of solute additions of titanium, titanium + niobium and phosphorus, were hot-dipped in a pure zinc (0.00 wt % Al) at 450 °C in order to study the morphology and kinetics of Fe–Zn phase formation. Uniform attack of the substrate occurred on all of the steels leading to the formation of a three-phase alloy layer morphology containing gamma, delta and zeta Fe–Zn phases. Titanium and titanium + niobium solute additions had no effect on the growth kinetics of any of the Fe–Zn phases. Phosphorus additions were found to retard only the kinetics of gamma-phase growth, without influencing the growth kinetics of the other Fe–Zn phases. In fact, the gamma-phase layer in the phosphorus-containing substrates was no longer discernable in light optical microscopy after 120 s immersion. The growth kinetics of the total Fe–Zn alloy layer (gamma + delta + zeta) was dominated by the growth of the zeta-phase layer which was in contact with liquid zinc during immersion in the zinc bath. The zeta-phase layer followed a two-stage growth process governed by $t^{1/3}$ kinetics. The delta-phase layer also exhibited two-stage growth with parabolic $t^{1/2}$ kinetics. The gamma phase followed $t^{1/4}$ growth kinetics, indicative of grain-boundary diffusion-controlled growth.

1. Introduction

Interstitial-free (IF) steels have been found to have a more reactive behaviour relative to other drawing quality steel alloys during zinc-coating processing. The reactive behaviour of IF steels can lead to difficulty in controlling the degree of alloying that occurs during post-dip annealing. Rapid reaction rates during hot-dip galvanizing and post-dip annealing can lead to overalloying and subsequent poor formability properties of the coating during press-forming operations [1]. In an attempt to understand Fe–Zn reaction mechanisms on IF steels, Hisamatsu [2] proposed that grain boundaries in IF steels are more thermodynamically active because they are essentially carbon free due to carbide and carbonitride formation that results from carbide-stabilizing additions of titanium and/or niobium. According to Hisamatsu, the nucleation of Fe–Zn phases first occurs where the Fe–Al inhibition layer (which forms at the steel/coating interface during galvanizing in aluminum-containing zinc baths) first breaks down, at a thermodynamically active steel substrate grain boundary.

Other investigators [3] have shown that substrate carbon content may influence galvanizing kinetics, such that higher levels of substrate carbon content acts to inhibit Fe–Zn phase growth. The high reaction rates associated with IF steel, specifically delta and zeta Fe–Zn phase growth, were related to their ultra-low carbon content [4]. Although most galvannealing research has been concerned with the effect of zinc bath alloying additions and low-carbon steel substrates only, limited research has been reported on galvanizing reaction kinetics of IF steels [5–7]. The objective of this paper is to report results of a systematic study on the morphology and kinetics of Fe–Zn alloy formation in a series of interstitial-free steels immersed in a pure zinc bath. A comparison paper, Part II [8], will report the kinetics of Fe–Zn phase growth during immersion in a 0.2 wt % Al–Zn bath.

2. Experimental procedure

The steel alloy materials used for this study were produced by BHP Steel in Port Kembla, Australia, and had the initial ingot composition listed in Table I. All the alloys were cold rolled to a final sheet thickness of 0.4 mm (84% cold worked). Each 0.4 mm sheet sample (3.8 cm × 25.4 cm) was recrystallization annealed in a tube furnace under a reducing wet 18% H_2–N_2 gaseous atmosphere at 815 °C for 15 min. After annealing, the samples were water quenched and prepared for galvanizing. The final carbon content of the annealed sheet samples (Table II) was determined by inert gas fusion chemical analysis. The average grain sizes of all the alloys was in the range of 10–20 μm.

0022–2461

TABLE I BPH sheet steel chemical analysis (10^{-4} wt %, or parts per million)

Steel alloy	C	Si	S	N	Al	Mn	P	Ti	Nb	B
LC	90	30	40	12	380	2580	20	80	< 50	< 3
LC–P	50	20	40	9	340	2690	600	60	< 50	< 3
TI IF	80	20	30	12	310	2590	30	750	< 50	< 3
Ti–P IF	60	50	20	10	390	2670	750	610	< 50	< 3
Ti–Nb IF	70	30	30	8	310	2470	40	330	210	< 3
Ti–Nb–P IF	60	50	30	9	330	2740	700	370	220	< 3

TABLE II Carbon content of IF steels after recrystallization annealing

Sample	Carbon content (wt %)
LC (ULC)	0.003
LC–P (ULC–P)	0.003
TI IF	0.006
Ti–P IF	0.004
Ti–Nb IF	0.003
Ti–Nb–P IF	0.004

The steel samples were pickled in a 10%–15% HCl acid solution to remove the thin oxide layer that formed during water quenching after recrystallization annealing. The samples were then immersed in an alkaline cleaning solution (80 °C) for 5 min, rinsed in water, pickled in a 10%–15% HCl acid solution for 30–60 s, rinsed in water again, and then immersed in a $NH_4Cl/ZnCl_2$ flux solution (70 °C) for 5 min. The steel samples were then dried in a vertical radiant tube furnace at 120 °C for 5 min immediately before immersion into the zinc bath.

All of the samples were zinc coated on a hot-dip galvanizing simulator. The simulator consists of three stations: (1) a vertical radiant tube furnace (120 °C), (2) a zinc melt box furnace (17 kg Zn bath, 450 °C), and (3) a water-quench tank. The simulator is equipped with an automated sample delivery system that allows for all of the processing steps to be performed sequentially at the same speed, in addition to maintaining a constant insertion and removal rate at each station. The horizontal traverse speed of the delivery system was 25.4 cm s^{-1}. This traverse speed allowed for the samples to be water quenched within 2.5 s after removal from the zinc bath, preventing zinc solidification before water quenching. The samples were inserted and removed at each processing station at a vertical speed rate 25.4 cm s^{-1}. Hot-dip galvanizing was conducted at 450 °C in a pure zinc, iron-saturated (0.03 wt % Fe) bath and individual samples with immersion times of 5, 10, 30, 60, 120 and 300 s were prepared.

All coated samples were sectioned transverse to the rolling direction of the sheet and prepared for metallographic examination as described elsewhere [9]. In order to quantify Fe–Zn alloy layer development, quantitative image analysis software was used on a LECO 2001 Image Analysis System. Individual alloy layers of gamma-, delta- and zeta-phases were identified within the total Fe–Zn layer as previously reported [9]. The individual layers were measured over five fields of data (ten measurements/field), at a magnification of $\times 1000$ and average and standard deviation values were calculated from the compiled individual phase-layer thickness data.

3. Results and discussion

3.1. Morphology of Fe–Zn phase formation in a 0.00 wt % Al–Zn bath

The formation and growth kinetics of the low-carbon (LC) steel has recently been reported [4]. The sequential nucleation of Fe–Zn phases occurs at the steel/coating interface in the following order: (1) zeta-phase, (2) delta-phase, and after some incubation time (3) gamma-phase, e.g. Fig. 1. The Fe–Zn phase layer development is also shown schematically in Fig. 2, where the sequence of reaction is represented chronologically. t_0 corresponds to zero time, and development occurs according to time such that $t_0 < t_1 < t_2 < t_3 < t_4$. Zeta, the most zinc-rich Fe–Zn phase to form at the steel/coating interface, nucleates first (t_1 in Fig. 2). The zeta layer nucleation is immediately followed by delta-phase formation (t_2) at the alpha Fe/zeta interface. There was no apparent delay in the formation of zeta or delta phases as both were found to form a continuous layer at the lowest reaction times, i.e. after 5 s reaction time. The gamma phase was found to form (t_3) after an incubation time of 30 s. The last morphological feature to develop in the 0.00 wt % Al–Zn bath was the formation of a second zeta layer ($zeta_2$) between 30 and 60 s reaction time (t_4) at the $zeta_1$/delta interface.

X-ray diffraction analysis of the gamma-, delta- and zeta-phase layers results in severe peak overlap, especially for the delta- and zeta-phases. Thus this type of analysis was not conducted for phase-identification purposes. In order to confirm individual phase-layer identification initially characterized by morphology in light optical microscopy (LOM), electron probe microanalysis for iron and zinc composition was determined at 1.0 μm increments across the total Fe–Zn alloy layer for the 10, 60 and 300 s immersion samples. An example of the iron concentration profile data for a 300 s immersion sample is plotted in Fig. 3. The iron composition data were found to correspond to what was observed morphologically, with gamma-, delta- and zeta-phase layer compositions (based upon the metastable Fe–Zn equilibrium [10]), and these composition data

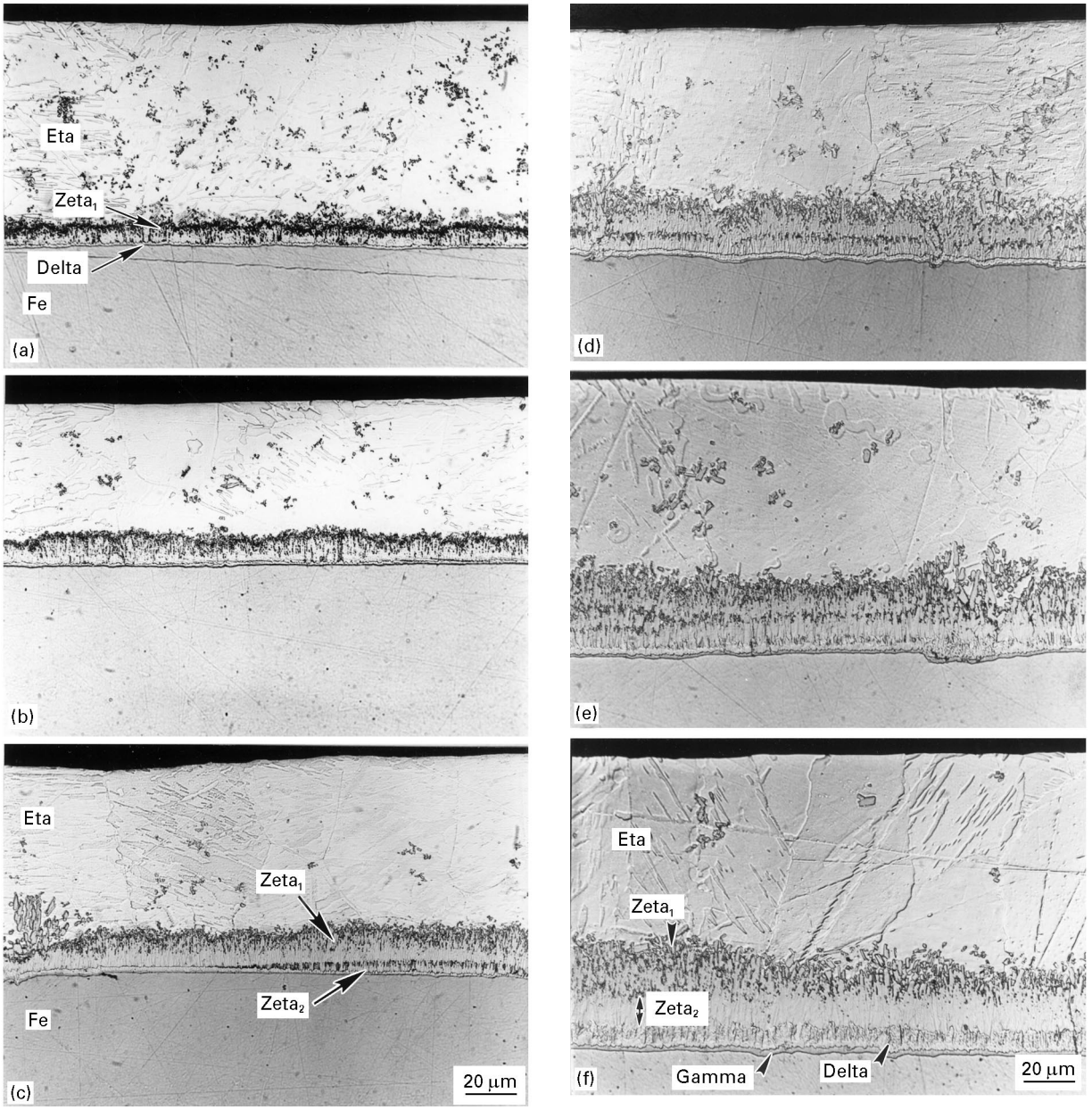

Figure 1 Ti IF steel hot-dip galvanized in a 0.00 wt % Al–Zn bath for (a) 5 s, (b) 10 s, (c) 30 s, (d) 60 s, (e) 120 s and (f) 300 s.

correlated with the measured individual layer-thickness data. No significant differences in the iron composition profiles were observed for the substrates studied. An example of a back-scattered electron (BSE) image (which shows atomic number contrast in a polished and unetched sample) of a total Fe–Zn alloy layer formed in a 0.00 wt % Al–Zn bath is shown in Fig. 4. The atomic number contrast visible in Fig. 4 confirmed the development of a three-phase Fe–Zn layer structure which was observed morphologically and identified by composition in the electron microprobe.

Microhardness testing was conducted on the substrate steel and individual Fe–Zn phase layers formed on the ULC steel sample immersed to 300 s to confirm further the Fe–Zn phase identification, especially between the delta- and zeta-phase layers. The 300 s immersion sample was chosen because relatively thick layers of delta- and zeta-phases could be analysed. The Vickers microhardness data are reported in Table III, and are in general agreement with trends reported for ferrite, and the Fe–Zn delta-, zeta- and eta-phases [11, 12]. The gamma-phase layer could not be evaluated because its layer thickness was too thin to be adequately tested at the smallest load (25 g) available on the microhardness tester.

The gamma-phase layer was found to disappear on all of the phosphorus-containing substrates after 120 s reaction. According to Horstmann [13], the gamma phase should form at the substrate alpha iron/gamma interface during the reaction between iron and zinc. The gamma-layer formation and growth appears to occur for reaction times between 30 and 300 s on the ULC, Ti IF and Ti–Nb IF steels. However, for the phophorus-containing steels, the growth of gamma layer occurs only up to 120 s reaction. After 120 s the rapidly growing delta-phase consumes the gamma-phase on the phosphorus-containing alloys as shown in Fig. 5 (arrows).

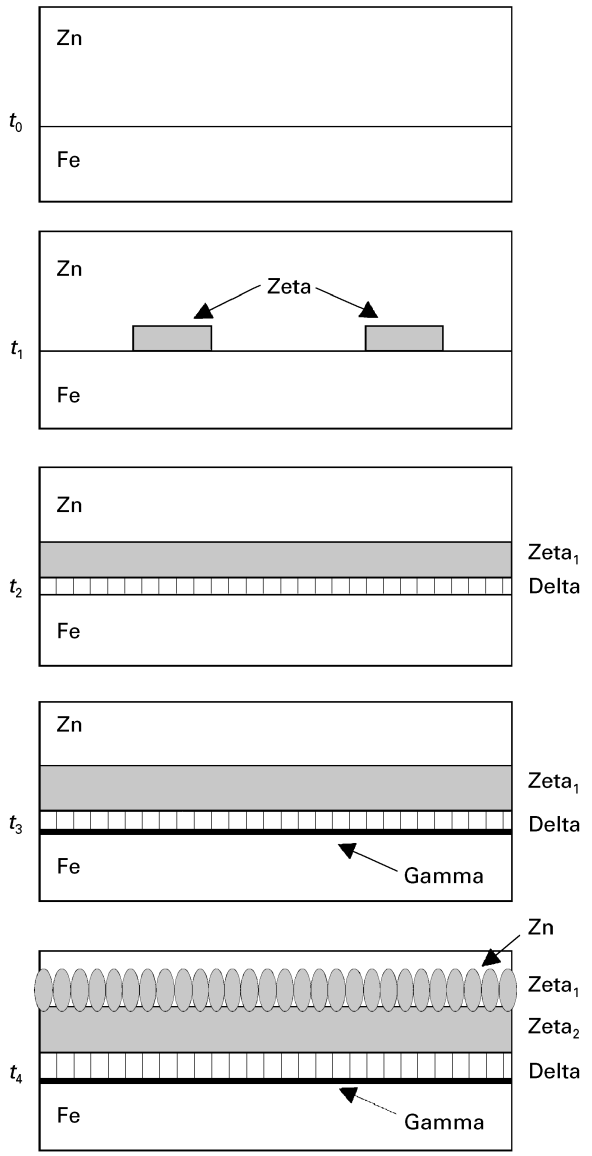

Figure 2 A schematic representation of Fe–Zn phase layer formation in a 0.00 wt % Al–Zn galvanizing bath. t_0 corresponds to zero time, and development occurs according to time, such that $t_1 < t_2 < t_3 < t_4$.

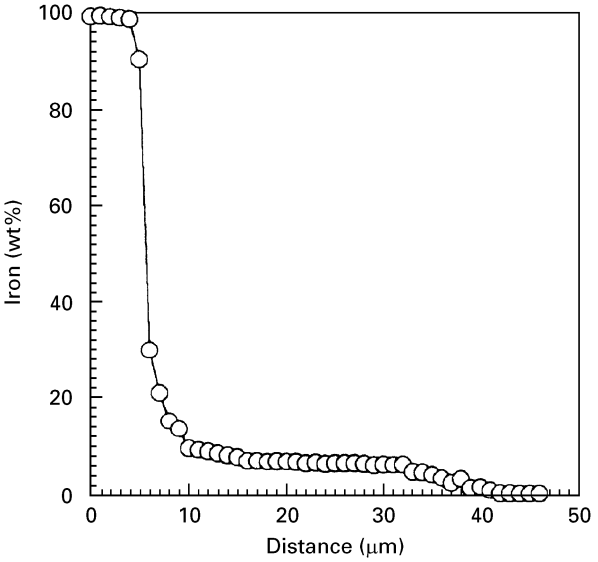

Figure 3 Iron concentration profile for the total Fe–Zn alloy layer formed on the Ti IF steel hot-dip galvanized in a 0.00 wt % Al–Zn bath for 300 s immersion.

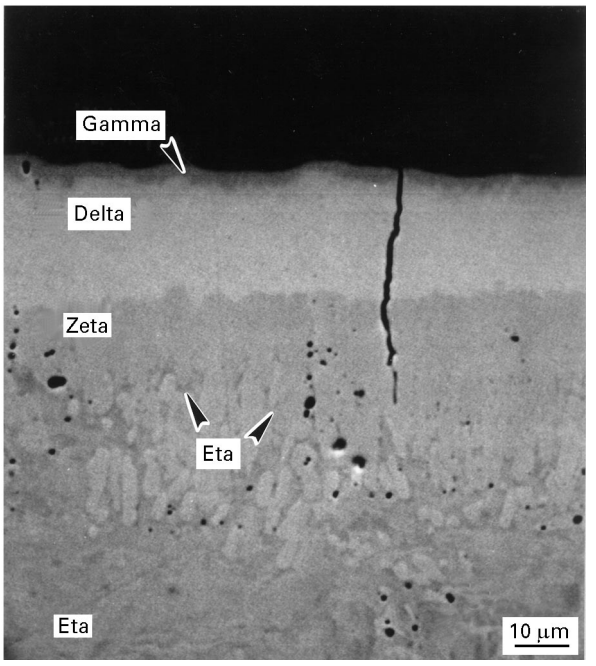

Figure 4 BSE image of the three distinct Fe–Zn phase layers formed on the 15 μm grain size ULC steel hot-dip galvanized in a 0.00 wt % Al–Zn bath for 300 s immersion.

TABLE III Vickers microhardness data of individual Fe–Zn phase layers and ULC substrate steel (25 g load, 15 s dwell time)

Layer	Average Vickers microhardness number
ULC Steel	85.7 ± 1.6
Delta-phase	273.2 ± 20.5
Zeta-phase	117.9 ± 9.0
Eta-phase	40.6 ± 4.7

3.2. Kinetics of Fe–Zn phase growth in a 0.00 wt % Al–Zn bath

The six interstitial-free steels were analysed to determine reaction kinetics during hot-dip galvanizing in a 0.00 wt % Al–Zn bath for 5–300 s immersion. The total Fe–Zn alloy layer or reaction layer was typically of a uniform thickness and its coverage at the steel/coating interface was complete. Fe–Zn total alloy layer development was similar on all of the steel substrates, and an example of Fe–Zn alloy layer development on the Ti IF steel substrate is shown in Fig. 1. The total Fe–Zn alloy layer thickness was measured for each reaction time studied, and the growth data for the six steel substrates are shown in Fig. 6.

To evaluate the kinetics of Fe–Zn alloy layer growth, a power-law growth equation

$$Y = Kt^n \tag{1}$$

was used to interpret the growth data where Y is the growth layer thickness, t is reaction time, K is a growth-rate constant, and n is the growth-rate time constant. By applying a logarithmic function on either side of Equation 1,

$$\log Y = \log K + n \log(t) \tag{2}$$

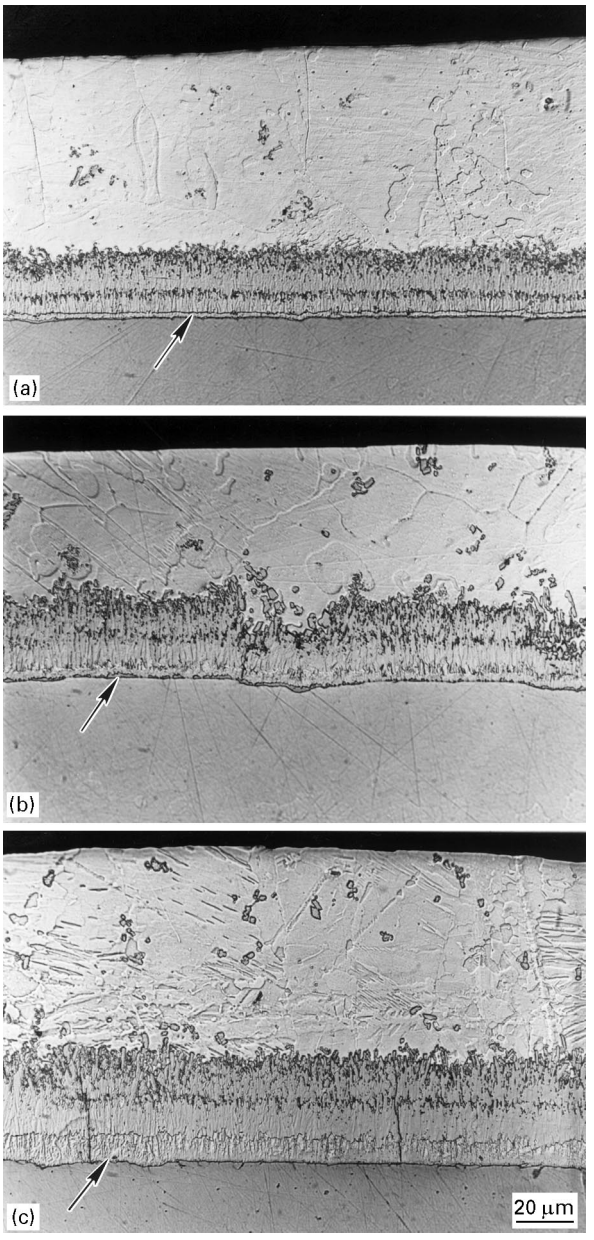

Figure 5 Ti–P IF steel hot-dip galvanized in a 0.00 wt % Al–Zn bath for (a) 60 s, (b) 120 s, and (c) 300 s immersion.

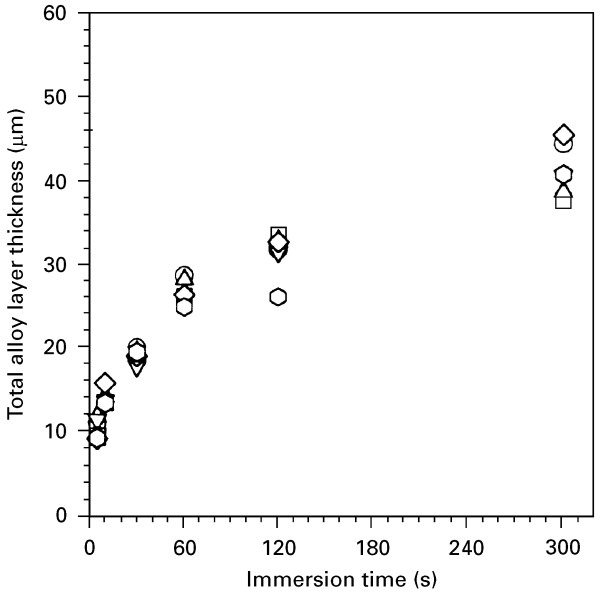

Figure 6 Total Fe–Zn alloy layer growth for substrate steels hot-dip galvanized in a 0.00 wt % Al–Zn bath: (○) ULC, (□) ULC – P, (△) Ti IF, (▽) Ti–P IF, (◇) Ti–Nb IF, (⬡)Ti–Nb–P IF.

TABLE IV Total Fe–Zn alloy layer growth-rate time-constant, n, values for steels hot-dip galvanized in a 0.00 wt % Al–Zn bath

Sample	Growth-rate time constant, n
ULC	0.35 ± 0.02
ULC-P	0.35 ± 0.03
Ti IF	0.31 ± 0.02
Ti–P IF	0.33 ± 0.02
Ti–Nb IF	0.37 ± 0.03
Ti–Nb–P IF	0.34 ± 0.03

and plotting the log value of the total alloy layer thickness, Y, as a function of the log value of immersion time in the bath, t, a line can be fitted to the data whose slope is n, the growth-rate time constant value [13], and whose y-intercept is log K, a log value of another growth rate constant. The growth-rate time constant, n, value is an indication of the type of kinetics controlling the growth of the layer under study. An n value of 0.5 is indicative of parabolic diffusion-controlled growth, while an n value of 1.0 is representative of linear kinetics in which growth is interface controlled.

The total Fe–Zn alloy layer was analysed to determine growth-rate time-constant values. The n values were determined from a linear regression analysis in the software program Sigma Plot (copyright Jandel Scientific) and are shown in Table IV. The n values were found to range from 0.31–0.37, and do not match a 0.50 value expected for parabolic volume diffusion-controlled growth. The total alloy layer growth instead followed a $t^{1/3}$ ($n \sim 0.33$) relationship.

Although the growth of the total Fe–Zn alloy layer did not follow a $t^{1/2}$ relationship, its growth was controlled by a steady-state diffusion process. For a steady-state diffusional growth process, plotting the concentration of iron in the total Fe–Zn alloy layer as a function of $x/t^{1/2}$ (where x is a distance parameter as measured from the estimated steel coating interface and t is reaction time) an invariant penetration plot over the reaction times studied should result. As shown in Fig. 7, the penetration curve was invariant for the Fe–Zn reaction layer formed at 10, 60 and 300 s reaction time on the ULC steel hot-dip galvanized in the 0.00 wt % Al–Zn bath. The penetration curves for the other steel substrates studied in this bath were also invariant over 10–300 s reaction time in the zinc bath. Onishi [14] has previously shown that in solid Fe–Zn diffusion couples annealed at 410 °C, in which molybdenum markers were placed at the original Fe/Zn interface, the markers were always found at the Zn/zeta-phase interface for reactions studied up to 100 h annealing time. Onishi *et al.*'s results indicate that one-sided diffusion of zinc through the Fe–Zn phases dominates the total alloy layer-growth rate, and the penetration curve in Fig. 7

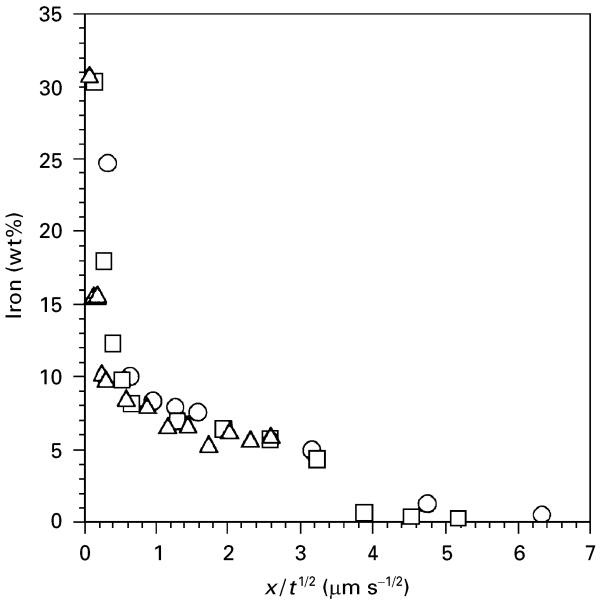

Figure 7 Iron concentration penetration curve for the 15 μm grain size ULC steel substrate hot-dip galvanized in a 0.00 wt % Al–Zn bath: (○) 10 s, (□) 60 s, (△) 300 s.

shows a steady-state diffusion process controls the total Fe–Zn growth reaction. One explanation for the observed $t^{1/3}$ growth kinetics is that the total alloy layer growth is controlled by diffusion along intermetallic Fe–Zn phase layer grain boundaries (such as along zeta-phase grain boundaries) instead of the bulk iron and zinc interdiffusion.

All of the substrate steels showed the development of a three-layer morphology of gamma-, delta- and zeta-phases, as shown in Figs 1 and 2. Zeta, the most zinc-rich Fe–Zn phase, formed first, followed sequentially by delta- and gamma-phase layers. The delta- and zeta-phase layers were present at all of the reaction times studied (5–300 s), whereas the gamma phase often had an incubation time of 30 s associated with its formation. Individual phase-layer growth was measured for gamma-, delta- and zeta-phase layers formed on each of the substrate steels studied, e.g. Fig. 8.

The zeta-phase layer was observed to contain a horizontal array of apparent voids formed within the zeta-phase layer after 30 s reaction time, e.g. Fig. 1. The voids distinguishing the two zeta-phase layers were found upon repolishing and back-scattered electron (BSE) imaging analysis of the unetched structure not to be voids but rather entrapped eta-phase (solidified zinc) (Fig. 4). The growth of the zeta layer was analysed as two separate layers: (1) $zeta_1$ which was defined as the layer adjacent to the delta layer before the entrapment of eta-phase, and (2) $zeta_2$ which formed at the $zeta_1$/delta interface after 60 s reaction time. The growth of the two zeta layers is presented in Fig. 9. The $zeta_1$ layer showed rapid growth from 5–30 s, then at 60 s the formation of the $zeta_2$ layer occurred and the $zeta_1$ layer then showed essentially no growth from 60–300 s reaction. The entrapped eta-phase between the two zeta layers remained at a constant distance from the Zn/$zeta_1$ interface.

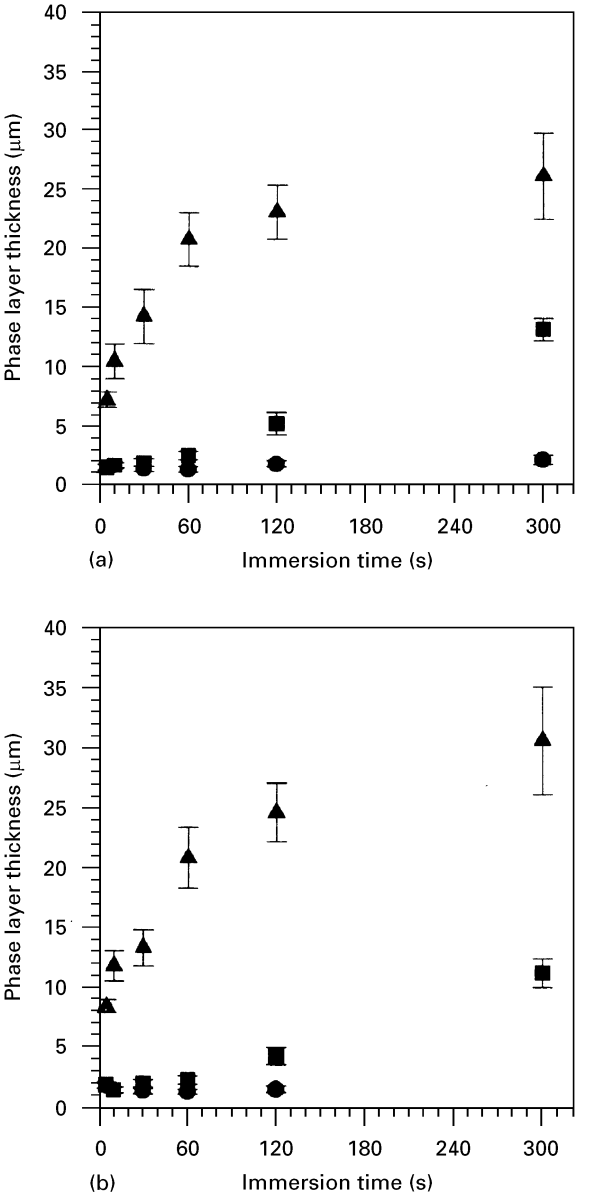

Figure 8 Individual Fe–Zn (●) gamma- (■) delta- and (▲) zeta-phase layer growth for the (a) ULC and (b) ULC-P steel substrates hot-dip galvanized in a 0.00 wt % Al–Zn bath.

Channels of liquid zinc were found to reach the $zeta_1$/delta phase by transport along the columnar structure of the $zeta_1$ phase layer. Therefore, the initial rapid growth (< 30 s) of the $zeta_1$ layer could occur according to linear interface-controlled kinetics. The growth of the $zeta_1$ layer changes over from linear to parabolic growth between 30 and 60 s. A 60 s reaction time corresponds to the time of $zeta_2$ layer formation at the $zeta_1$/delta interface and also to the point at which entrapped eta-phase regions were found to form. Van Loo and Rieck [15] found a similar reaction-layer morphology in a $TiAl_3$ layer formed between titanium and aluminium in a solid Ti–Al diffusion couple, where aluminium was the dominant diffusing species. The $TiAl_3$ layer developed an internal horizontal array of pores which remained at a constant distance from the Al/$TiAl_3$ interface. Van Loo and Rieck also found the initial linear growth reaction to be difficult to determine due to the short time of duration (a few hours). In the Fe–Zn system the

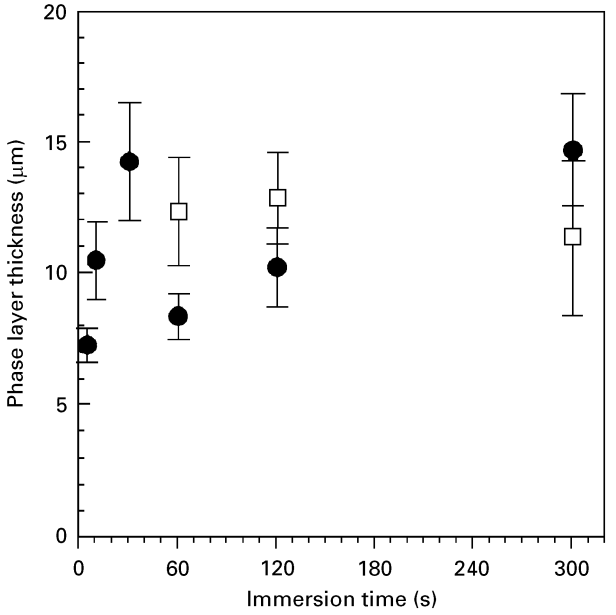

Figure 9 Separate (●) $zeta_1$- and (□) $zeta_2$-phase layer growth for the ULC steel hot-dip galvanized in a 0.00 wt % Al–Zn bath.

TABLE V Individual Fe–Zn phase layer growth-rate time-constant, *n*, values for the steels hot-dip galvanized in a 0.00 wt % Al–Zn bath

Sample/layer	Growth-rate time constant, *n*
Gamma-phase layer	
ULC	0.24 ± 0.06
ULC–P	0.10 ± 0.08
Ti IF	0.22 ± 0.11
Ti–P IF	0.035 ± 0.080
Ti–Nb IF	0.23 ± 0.05
Ti–Nb–P IF	0.13 ± 0.28
Delta-phase layer	
ULC	0.51 ± 0.11
ULC–P	0.44 ± 0.12
Ti IF	0.34 ± 0.12
Ti–P IF	0.37 ± 0.13
Ti–Nb IF	0.44 ± 0.15
Ti–Nb–P IF	0.39 ± 0.15
Zeta-phase Layer	
ULC	0.32 ± 0.03
ULC–P	0.32 ± 0.03
Ti IF	0.28 ± 0.05
Ti–P IF	0.29 ± 0.03
Ti–Nb IF	0.33 ± 0.05
Ti–Nb–P IF	0.33 ± 003

possible observed linear growth duration for the $zeta_1$ phase layer was approximately 5–30 s; however, its kinetics were also difficult to define as linear because of the limited number of data points.

In the case of the liquid–solid diffusion couple analysed here, the zeta layer grows linearly up to a critical thickness (10–15 μm) which occurred after 30–60 s reaction time. After this initial growth, further growth of the zeta-phase layer may become unstable due to growth stresses that have developed within the zeta layer. The surface contact of the zeta layer with the liquid zinc may keep the outermost columnar structure of the zeta-phase in tension, and thus allows for liquid zinc penetration along the columnar zeta layer and reaction at the zeta/delta-phase interface. After liquid zinc reaches the zeta/delta interface, a new zeta layer ($zeta_2$) formed. The first zeta layer that formed ($zeta_1$) did not show growth after 30 s. As stated earlier, 60 s reaction was the time at which both the formation of entrapped eta occurred and the delta-layer growth accelerated as the total zeta-layer growth slowed. In the Fe–Zn system, gamma- and delta-phase layers are formed in addition to the zeta-phase layer, and the rapid growth of the adjacent delta layer must also be considered in how it affects the zeta-layer growth pattern.

The individual $zeta_1$ and $zeta_2$ growth layers could not be analysed to determine the growth-rate time constant (*n* value) of each layer due to a lack of data on either side of the 60 s transition point. Therefore, more data before and after 60 s reaction time are needed accurately to fit the two-stage growth of the zeta-phase layer. It was found that the zeta-phase layer could be more accurately evaluated for its growth behaviour as one layer, thus zeta-phase layer-growth analysis was conducted on the total zeta layer ($zeta_1 + zeta_2$) and includes the entrapped eta-phase in the layer-thickness measurements. The zeta-phase layer-thickness data were then fit to determine growth-rate time-constant, *n* values, which are listed in Table V. Growth-rate time-constant values range from 0.28–0.33, thus the total zeta-layer kinetics also followed a $t^{1/3}$ relationship, as was the case for the total Fe–Zn alloy layer (Table IV).

Coarsening of the zeta-phase could account for the observed $t^{1/3}$ growth followed by the total zeta layer. Coarsening and grain growth during phase-layer growth, where grain-boundary diffusion occurs, has been shown to follow $t^{1/3}$ kinetics [16] for the Cu_6Sn_5 phase formed between a molten Pb/Sn solder and a thin Cu_3Sn phase grown on a copper substrate. Copper was the dominant diffusion species, and the Cu_6Sn_5 phase was able to grow due to (1) copper diffusion into the liquid channels of the solder, and (2) copper diffusion into the growing Cu_6Sn_5 grains. The flux of copper atoms also resulted in a coarsening of the Cu_6Sn_5 phase, thus causing a reduction in the liquid solder channel area, and the kinetics of growth for the Cu_6Sn_5 phase followed a $t^{1/3}$ relationship. A similar mechanism of zinc diffusion and a flux of zinc atoms supplying the growing zeta-phase layer may have resulted in a coarsening of the zeta-phase layer structure in the present research. Fig. 1d–f show that the width of the columnar features of the zeta-phase have increased with reaction times, indicating some coarsening may have occurred during growth.

For grain-boundary diffusion in the presence of a compound layer, enough material must be delivered to the growth interface along grain boundaries [17]. If the grain size of the reaction layer increases, then growth can occur according to less than parabolic ($n < 0.5$) kinetics. Any mechanism that results in appreciable loss of a material from a growing layer or

a time-dependent reduction of the flux of material to the growth interface, can also result in non-parabolic growth behaviour. Material from a reaction layer could be lost due to dissolution. In the Fe–Zn system, the dissolution or consumption of the zeta-phase by the delta-phase layer is possible. From grain-boundary diffusion, non-parabolic behaviour can also result from a time-dependent reduction in the flux to the growth interface, due to an increase in grain size of the reaction layer or to reduction in the number of high diffusivity paths between the source and the growth interface.

Phosphorus and other solute additions to the substrate steel would generally be thought not to have a significant influence on zeta-phase layer growth because substrate steel solute additions should not affect the diffusion of zinc across the zeta-phase layer. Owing to the fact that the zeta layer is located at a distance of approximately 2–20 μm from the steel/coating interface and that it is not in direct contact with the substrate steel, its growth rate should not be directly affected by substrate chemistry. Dramatic changes in delta-phase layer growth rate on one side of the zeta-phase layer, and/or changes in the ability of liquid zinc to penetrate the zeta-phase layer (for example, coarsening of the zeta-phase columnar structure) would be the only significant factors affecting zeta-layer growth.

The delta-phase layer, like the zeta-phase layer, showed a two-stage growth development for all substrates, with a transition in growth occurring at 60 s reaction time (e.g. Fig. 8). After immersion, the delta layer had little or no growth up to 60 s, and thereafter delta-layer growth was rapid. At 60 s immersion time, liquid zinc was able to penetrate the zeta-phase layer and react with the delta-phase layer, thus resulting in an increased rate of growth of the delta-phase. The delta-phase layer appeared to grow at the expense of the zeta-phase layer because 60 s reaction time was also the point at which entrapped eta was found to develop within the zeta-phase layer, and its growth rate slowed. The delta-phase layer growth data were also analysed for growth-rate time-constant, n, values according to a power-law growth relationship, and the values are listed in Table V. The n values range from 0.35–0.51 but have a large error, which was associated with the two-stage growth of the delta-phase layer. Overall, the delta-layer growth followed a close to $t^{1/2}$ relationship, and this growth was similar on all of the substrate steel alloys studied.

The gamma-phase layer was first observed at 30 s reaction time on all of the substrate steels studied. Phosphorus-containing substrates showed a disappearance of the gamma layer at 300 s reaction time as previously described, Fig. 5. The gamma-layer thickness data were first fit to determine n values over the corresponding reaction time ranges at which an interfacial gamma layer was observed on each individual substrate steel. The n values are listed in Table V. Growth-rate time-constant, n, values for the ULC, Ti IF and Ti–Nb IF steel alloys were between 0.22 and 0.24, and were within the error values of one another, indicating gamma-layer growth followed

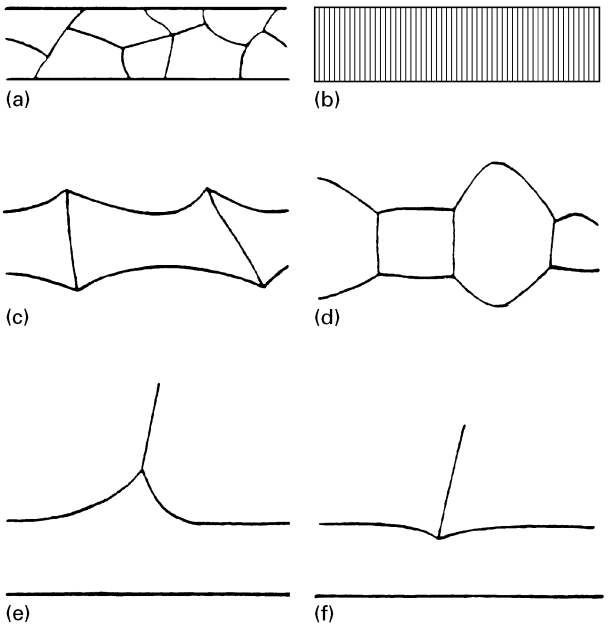

Figure 10 Various morphologies of a reaction layer in a binary diffusion couple: (a) volume diffusion, (b), (c) and (e), (f) grain-boundary diffusion, and (d) growth along a preferred crystallographic direction, controlled processes [11].

a $t^{1/4}$ relationship. The n values for the phosphorus-containing alloys ranged from 0.035–0.13 and had a large error associated with their values due to the disappearance of the gamma phase at 300 s, and to the reduced number of data points over which the data could be fitted. Although the error was large for the growth-rate time-constant, n, values determined from the phosphorus-containing alloys, phosphorus substrate solute additions were found significantly to retard the kinetics of gamma-phase layer growth, most likely by blocking zinc diffusion down substrate grain boundaries as proposed by Allegra *et al.* [18].

The gamma-phase layer may have had a morphology indicative of grain-boundary diffusion-controlled growth similar to that shown in Fig. 10e and f [19]. The limiting mechanism of the grain-boundary diffusion of zinc for gamma-phase growth could be due to the recrystallization of the gamma layer during the galvanizing reaction at 450 °C. In this study, it was not possible to distinguish between gamma- and gamma_1 phases at the interface. However, the gamma_1 phase has typically been found to form as a distinct layer between the delta and gamma-phases after long-term annealing in solid Fe–Zn diffusion couples [11] or at elevated temperatures of annealing, such as 500–550 °C [20, 21], thus the gamma-phase layer studied here is most likely not the gamma_1-phase. Adachi *et al.* [22], however, found that grain growth did not occur in the gamma-phase during annealing at 500 °C; therefore, it most likely did not occur in this study during galvanizing at 450 °C. Recrystallization and grain growth of the gamma layer therefore do not account for the observed $t^{1/4}$ kinetics of growth of the gamma-phase layer during galvanizing. Possibly the growth of the delta-phase layer also influences the growth of the gamma-phase. The migration of the delta-phase has been found to occur in two directions,

both toward the zinc melt and zeta-phase layer, as well as toward the substrate steel and gamma-phase layer [13]. The consumption of the gamma-phase by the rapidly growing delta-phase layer may best explain the non-parabolic growth behaviour of the gamma-phase layer.

Summarizing the kinetics observed for the Fe–Zn phase layers formed in the 0.00 wt % Al–Zn coatings, the total Fe–Zn alloy layer as well as the individual phase layers did not follow parabolic or linear parabolic kinetics. Initially the zeta-phase layer grows rapidly up until 60 s reaction time, while the delta- and gamma-phase layers showed little or no growth during the same time of reaction (Fig. 8). However, from 60–300 s reaction time, zeta and gamma-layer growth rates slowed, and delta-layer growth accelerated. The zeta- and gamma-phase layers for all substrates were found to have growth kinetics following $t^{1/3}$ and $t^{1/4}$ relationships, respectively, indicating their growth may follow grain-boundary diffusion-controlled growth. That both zeta- and gamma-phase layers show growth–time relationships less than $t^{1/2}$, indicates that the supply of zinc to these growth layers is reduced as a function of time.

The reduction of zinc supply through the zeta layer could be due to coarsening of the zeta-phase columnar structure during diffusional growth. As the width of the zeta-phase columnar structure increases during the reaction, less columnar boundary area is available for fast diffusion of liquid zinc, and the zinc supply becomes limited as liquid channels of zinc in contact with the zeta layer become narrower and are eventually blocked by the growth and coarsening of the zeta-phase layer itself. The zeta-phase has a columnar needle-like morphology (Fig. 1) indicative of a type of morphology found for grain-boundary diffusion-controlled kinetics [19], as shown in Fig. 10b.

The total Fe–Zn alloy layer had a growth-rate time-constant, n, value of 0.33 while the gamma layer had an average n value (for the non-phosphorus-containing substrates) of 0.25, the delta-phase layer n value was approximately 0.33–0.50, and the zeta layer had the same growth-time relationship as the total Fe–Zn alloy layer with an average n value of 0.33. The n values determined from the individual phase layers are in agreement with the n values reported previously in the literature of 0.25, 0.50 and 0.35 for the gamma-, delta- and zeta-phase layers, respectively [23]. Phosphorus solute additions were found to retard gamma-phase layer kinetics only, and showed no effect on delta- and zeta-phase growth. Titanium and niobium solute additions showed no significant effect on the kinetics and rate of Fe–Zn phase layer growth in the 0.00 wt % Al bath. The growth kinetics of the zeta-phase layer dominated the kinetics of the total Fe–Zn alloy layer as both were found to follow a $t^{1/3}$ growth relationship.

4. Conclusions

From this study of Fe–Zn phase formation in IF steels hot-dipped at 450 °C in a 0.0 wt % Al–Zn bath, the following conclusions can be drawn.

1. Uniform attack of the substrate steel leads to the development of a three-phase Fe–Zn alloy layer containing gamma-, delta- and zeta-phases. Zeta was the first zeta Fe–Zn phase to form, followed by delta- and then gamma-phase.

2. Phosphorus solute additions to ultra-low-carbon steel and interstitial-free steel were found to retard the kinetics of Fe–Zn gamma-phase layer growth, but did not affect the growth kinetics of any other Fe–Zn phases. Titanium and titanium + niobium solute additions had no effect on the growth kinetics of individual Fe–Zn phase layers present in the coating.

3. The growth kinetics of the total Fe–Zn alloy layer followed that of the zeta phase, indicating that the specific Fe–Zn phase layer in contact with the liquid zinc during galvanizing (zeta-phase) controlled the growth kinetics of the total Fe–Zn alloy layer. The zeta-phase layer followed a two-stage growth process with its overall growth governed by $t^{1/3}$ kinetics. The delta-phase layer also showed two-stage growth, with delta-phase following parabolic $t^{1/2}$ growth kinetics after an initial period of no growth. The gamma-phase grew according to $t^{1/4}$ kinetics, which is indicative of grain-boundary diffusion-controlled growth.

Acknowledgements

The authors thank A. O. Benscoter for his guidance in metallography. The helpful discussions with Professor M. Notis, Lehigh University, and Professor F. van Loo, Eindhoven Technical University, are gratefully acknowledged. In addition, the sponsorship of Cockerill Sambre (Michel Dubois), BHP Steel (Peter Mercer) and Union Miniere (Jean Wegria) is gratefully acknowledged.

References

1. A. R. MARDER, in "International Symposium on IF Steel Sheet Processing", 30th Annual Conference of Metallurgists, Canadian Institute of Mining, Metallurgy and Petroleum, Montreal, edited by C.E. Cullins and D.L. Barager, Ottawa, Canada (1991) p. 157.
2. Y. HISAMATSU, in "GALVATECH '89" edited by Y. Hasimatsu (ISIJ, Tokyo 1989) p. 3.
3. A. NISHIMOTO, J. INAGAKI and K. NAKAOKA, *Trans. ISIJ* **29** (1989) 3.
4. C. E. JORDAN and A. R. MARDER, in "GALVATECH '95", edited by J.E. Hartmann (Iron and Steel Society, Warrendale, PA, 1995) p. 319.
5. T. TOKI, K. OSHIMA, T. NAKAMORI, Y. SAITO, T. TSUDA and Y. HOBO, in "The Physical Metallurgy of Zinc Coated Steel" edited by A. R. Marder (TMS, Warrendale, 1994) p. 169.
6. C. E. JORDAN and A. R. MARDER, *ibid.* p. 197.
7. C. COFFIN and S. W. THOMPSON, in "GALVATECH '95", edited by J.E. Hartmann (Iron and Steel Society, Warrendale, PA, 1995) p. 121.
8. C. E. JORDAN and A. R. MARDER, *J. Mater. Sci.* **32** (1997) 5603–5610.
9. C. E. JORDAN, K. M. GOGGINS, A. O. BENSCOTER and A. R. MARDER, *Mater. Charact.* **31** (1993) 107.
10. P. PERROT, J.-C. TISSIER and J.-Y. DAUPHIN, *Z. Metallkde* **83** (1992) 11.
11. G. F. BASTIN, F. J. J. VAN LOO and G. D. RIECK, *ibid.* **65** (1974) 656.

12. M. GUTTMANN, *Mater. Sci. Forum* **155–156** (1994) 527.
13. D. HORSTMANN, "Reactions Between Iron and Molten Zinc" (Zinc Development Association, London, 1978)
14. M. ONISHI, Y. WAKAMATSU and H. MIURA, *Trans. JIM* **15** (1974) 331.
15. F. J. J. VAN LOO and G. D. RIECK, *Acta Metall.* **21** (1973) 61.
16. H. K. KIM and K. N. TU, *Phys. Met. Rev. B.*, **53** (1996) 16027.
17. H. H. FARRELL and G. H. GILMER, *J. Appl. Phys.* **45** (1974) 4025.
18. L. ALLEGRA, R. G. HART and H. E. TOWNSEND, *Metall. Trans.* **14A** (1983) 401.
19. F. J. J. VAN LOO, *Prog. Solid State Chem.* **21** (1990) 47.
20. C. S. LIN, W. A. CHIOU and M. MESHII, in "The Physical Metallurgy of Zinc Coated Steel", edited by A. R. Marder (TMS, Warrendale, PA, 1994) p. 31.
21. L. ESPERANCE, J. D. L'ECUYER, A. SINARD, M. P. BARRETO and G. BOLTON, in "GALVATECH '92" edited by Centre de Recherches Metallurgiques (Verlag Stahl Eisen, Dusseldorf, 1992) p. 442.
22. Y. ADACHI, T. NAKAMORI and K. KAMEI, GALVATECH '95 edited by J. E. Hartmann (Iron and Steel Society, Warrendale, PA, 1995) p. 471.
23. J. MACOWIAK and N. R. SHORT, *Int. Metals Rev.* **1** (1979) 1.

Received 3 March
and accepted 29 May 1997